Experimental study of a millimeter-sized Ga-In drop ablated by a nanosecond laser pulse

Yanchu Liu[1], Lihao Gao[1,2], Tianqi Zhai[1], Chenghao Xu[1], Hui Tang[2], Weiwei Deng[1, 3, *]

[1] *Department of Mechanics and Aerospace Engineering, Southern University of Science and Technology (SUSTech), Shenzhen 518055, China*

[2]*Department of Mechanical Engineering, The Hong Kong Polytechnic University, Hong Kong, China*

[3]*SUSTech Center for Complex Flows and Soft Matter Research, Shenzhen 518055, China*

* Corresponding author.

E-mail address: dengww@sustech.edu.cn

Abstract

The motion of millimeter gallium-indium (Ga-In) drops subject to intense Neodymium-doped Yttrium Aluminum Garnet (Nd: YAG) laser blasts in air is investigated experimentally. The drop first experiences plasma emissions and then undergoes interfacial instabilities. The effective ablation pulse energy is quantified by the laser-induced shockwave propagation. The laser-blast-induced concave expansion and spanwise depression history is measured, and the data collapse on straight lines with proper rescaling of pulse energy and time. The propulsion speed of the drop is described by a semi-empirical model that considers the laser energy and fluence at the threshold of ablation. The data shows that this propulsion speed scaling remains valid to the millimeter drop ablated by the pulsed laser with beam spot much smaller than the drop, although the original scaling was derived and verified for the indium-tin (In-Sn) droplet of tens of micrometers impacted by a laser pulse with the focal point larger than the droplet.

Keywords: laser ablation, drop, shock wave, interfacial instability, Ga-In, plasma propulsion

I. Introduction

The impact of a high energy short laser pulse on an opaque material can generate a rapid blow-off of high-temperature plasma at the target surface, which induces a momentum against the surface of this material. Subsequently, a strong shockwave is formed both inside[1] and outside[2] the material. Understanding the dynamics driven by laser ablation is critical[3], because this fast and complex process can be encountered in a wide range of applications. For instance, the research of the Rayleigh-Taylor instability (RTI) evolution in supernovae at astrophysical-scale is carried out based on the ablative plasma produced by a large laser facility in scale-invariant conditions[4]. In the direct-drive inertial confinement fusion (ICF) [5-7], many intense laser beams focused on spherical capsule surface produce ablation pressure to drive the deuterium-tritium-contained capsule to implode[8]. The fluid dynamics driven by laser ablation also have practical applications, such as the deformation and fragmentation of Sn microdroplet driven by laser induced plasma in the extreme-ultraviolet (EUV) light source in nanolithography[9, 10]. Many studies have been devoted to the interaction of laser with the targets. The laser ablation regime[11], ablation mechanism[12], ablation thresholds[13, 14], ablation depth, mass ablation rate[15, 16], concentration of plasma plumes[17] and the structure of laser ablation fronts have been investigated extensively at various laser intensities, wavelengths and durations of pulses[15, 18].

The laser-drop interaction is a subject of particular interest. After the ablation of a nanosecond laser pulse, the surface of the drop is compressed [19] and the drop spreads out, sometime even into a liquid sheet[20], which later on breaks into ligaments and

smaller drops[1, 21]. Until now, most researchers focus on the rim breakup and the sheet breakup after the significant deformation of the drop at tens of micrometer scale [21-23] . The droplet deformation and fragmentation processes have also been extensively studied[23-28]. However, very few fundamental studies related to laser-ablation-induced surface instability of a liquid drop exist [21, 29]. Although both dyed-water[19, 20, 30, 31] and liquid metal[9, 21, 24-27, 32] drop have been studied, we are more interested in the ablation process of the liquid metal drop because of its relevance in important technical applications such as ICF and EUV light source [9, 10].

Here, we present an analysis of the response of liquid Ga-In drops of millimeter scales to a 9-ns laser-pulse. The instability of the drop surface upon laser ablations is visualized. The shockwave generated by the laser-drop interaction is similar to that caused by a blast, hence the effective initial energy at the ablation center can be estimated based on the Taylor blast model[33]. We obtain the displacement of mass center from image sequences of the subsequent drop deformation process and find that the relationship between millimeter-sized drop propulsion speed and laser pulse energy is similar to that of droplet at dozens of micrometer scale[30, 32]. We show that the semi-empirical laser ablation propulsion model[24] derived for the ~100 μm liquid metal droplet in the literature is also applicable to the millimeter-sized drop, despite the vast difference in pressure distribution.

II. Experimental Methods

The experimental setup is shown schematically in Fig.1. Drops of Ga-In alloy (70Ga-30In of 99.999% purity with density ρ_m = 6.33 g/cm^3 at 20 ℃) are generated by

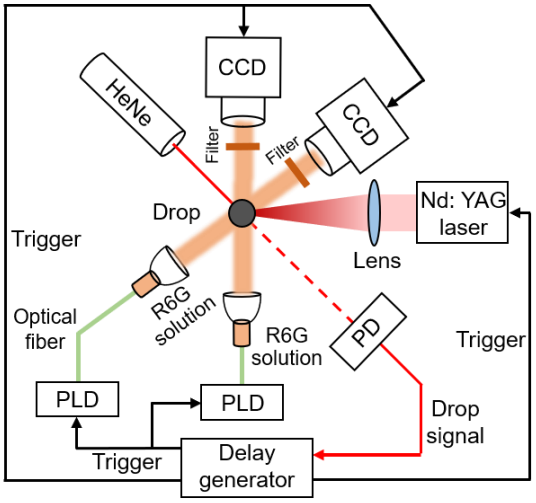

FIG. 1. Schematic of the experimental setup (top view). The drop is generated from a capillary tube connected to a reservoir of liquid metal, which is driven pneumatically. A horizontal continuous helium-neon (HeNe) laser beam and a photodiode (PD) form a photo-electric gate. The falling drop triggers a signal that is fed to a delay generator, which controls the rest of the equipment synchronously. The high energy laser is Nd: YAG with a duration of 9 ns FWHM at the wavelength of λ=1064 nm. The laser beam is focused by a 250-mm focal-length plano-convex lens into a 400 μm Gaussian spot on the surface of the drop. The light sources for imaging the drop are two Rhodamine 6G fluorescent solution pools excited by 5-ns 532 nm pulsed laser diodes, which emit 560 nm fluorescence. The two light sources are aligned at 45° and 90° to the Nd: YAG laser beam respectively. The light source projects shadowgraph that is recorded by the charge coupled device (CCD) camera combined with a long-distance microscope. A bandpass filter is used to suppress the plasma radiation and protect the imaging sensor.

pneumatically pumping the alloy through a capillary with an outer diameter of 260 μm. The drop has an equivalent spherical diameter of D_0 = 2.25(±0.05) mm. The released drops pass through a horizontal focused HeNe laser beam. The change in light intensity is detected by a photodiode that generates a step signal to trigger the Nd: YAG laser, which produces a laser pulse at λ =1064 nm wavelength with a duration of τ_p =9 ns full width at half maximum (FWHM). The Gaussian laser beam is focused to a diameter of 400 μm by a plano-convex lens. The energy of the laser pulse is varied between 36 and 427 mJ. The Ga-In alloy was chosen in this work because the 70Ga-30In alloy (melting point 16 ℃) is liquid at room temperature, therefore additional heating is not required.

Moreover, 70Ga-30In is not toxic (unlike mercury) and inexpensive.

The detailed information of the drops in the first microseconds after the laser impact is captured by the shadowgraph imaging systems, which consist of two long-distance microscopes (each paired with a high-speed camera), and 5-ns incoherent light source, which is based on the Rhodamine 6G fluorescent dye solution pumped by 5 ns 532 nm pulsed laser diodes (PLD). One of these microscopes has optical axis aligned orthogonally to the Nd: YAG laser beam to provide side-view images. The other one is angled at 45° to the beam direction for a tilted side view. A bandpass filter is placed in front of each microscope lens to suppress the plasma radiation. Stroboscopic time series of different drops are recorded by increasing the time delay between the shadowgraph systems and the Nd: YAG laser ablation. The high-speed camera (iSpeed 220) has a full frame resolution of 1600×1600 pixels. The resolving power is 3.4 μm/pixel for both the orthogonal and 45° shadowgraphs. The phenomena about 100 μs after the laser ablation is captured by another high-speed camera operated at 82802 frames per second (fps) illuminated by a continuous light source.

III. Results and discussion

The response of the Ga-In drop to the laser ablation with different pulse energies is shown in Fig. 2 (multimedia view). A plasma is generated at the ablation front as the laser impacts the drop surface and maintains the pressure to propel the drop, which happens in a scale of $\tau_a = 10^{-8}$~10^{-7} s. [34] As shown in Fig. 2(b) (multimedia view), a larger plasma is generated with a higher laser pulse energy and the plasma illumination is captured at 11 μs, which means the plasma exists for a longer duration. A shockwave

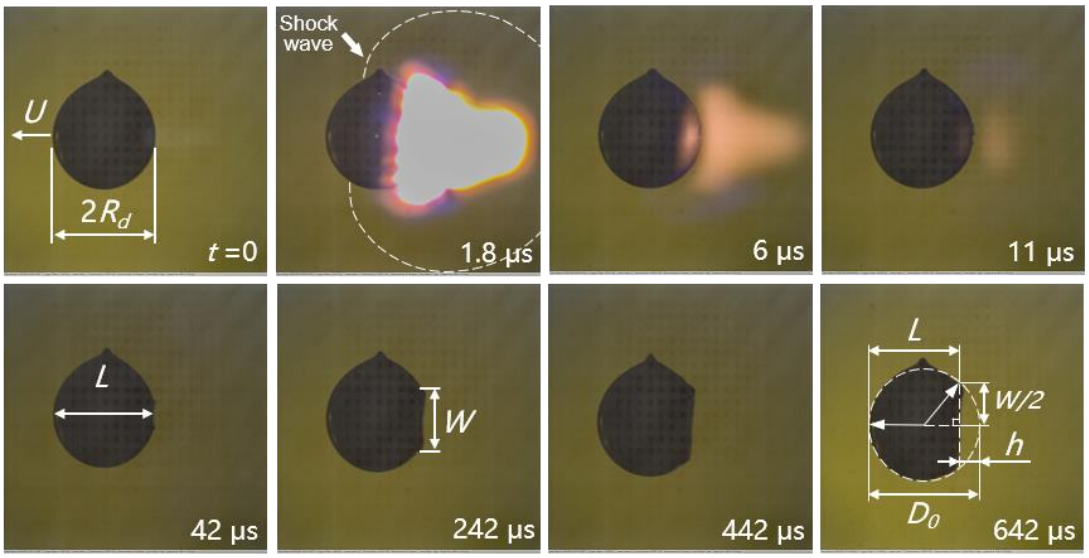

(a)

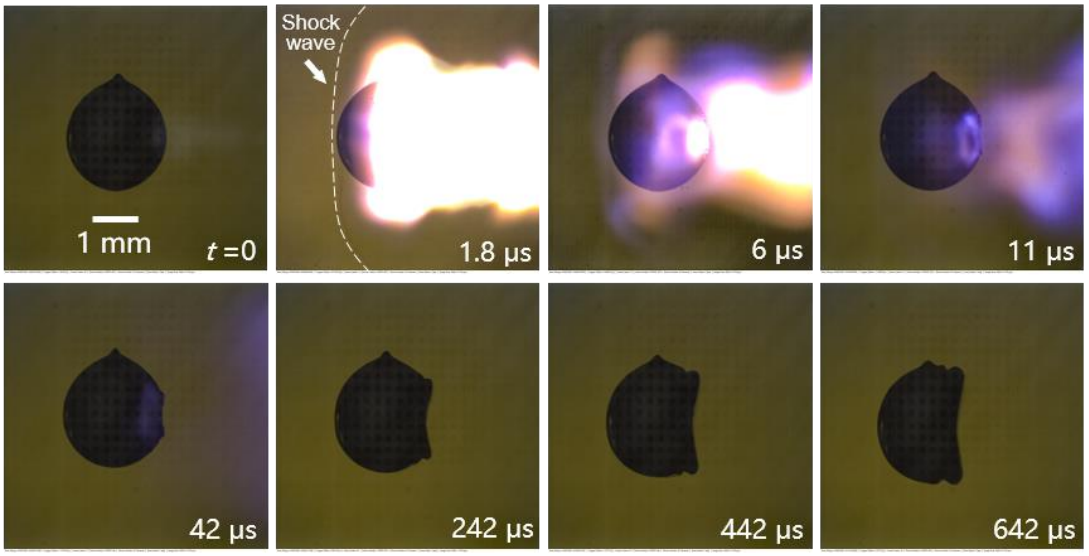

(b)

FIG. 2. Stroboscopic shadowgraph images of Ga-In drops taken before and after the laser ablation in the side view at different time delays for two laser-pulse energies. (a) The dynamics of a drop shape ablated by a 9-ns Nd: YAG laser pulse (pulse energy: 108 mJ, focal spot size: 400 μm). The bright light at the right side of the drop is plasma, which is generated as the laser ablates the surface of the drop. The liquid surface is pushed backward by the plasma pressure while the drop is propelled forward (multimedia view). (b) The same as (a) but with a pulse energy of 400 mJ, which leads to a brighter and wider plasma as well as more drop deformation (multimedia view).

forms and subsequently expands beyond the plasma. The plasma pressure pushes the surface of the drop into a concave, the diameter and depth of which grow over time with a rim forming at the edge of the depressed region. The deformation of the drop

occurs on the inertial time scale $\tau_i = R_d / U \sim 10^{-4}$ s and slows down under the surface tension with the capillary time scale $\tau_c = \sqrt{\rho_m R_d^3 / \sigma} \sim 10^{-3}$ s, where R_d is the equivalent spherical radius, U is the propulsion speed of the drop, and σ is the surface tension of Ga-In alloy. The complete response of the drop to the laser ablation involves four distinct time scales:

$$\tau_p < \tau_a \ll \tau_i < \tau_c. \tag{1}$$

Figure 3 shows the comparison of the interface deformation with different laser pulse energies captured as soon as it is visible. There are concentric circular ripples around the laser focal point for all laser pulse energies. Both the area of the rippled surface and the amplitude of the wave increase with higher laser pulse energy.

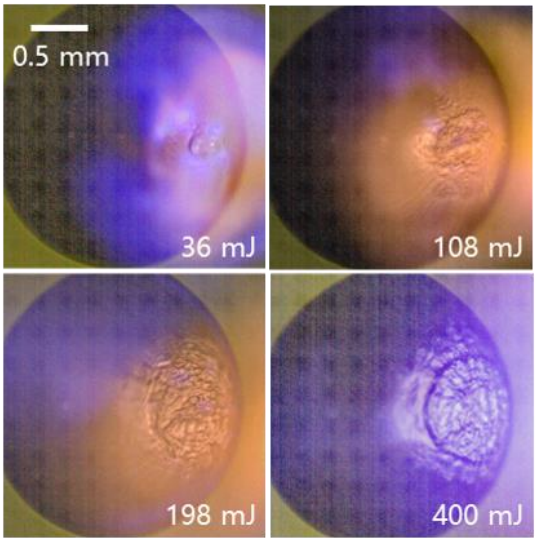

FIG. 3. Front-side view of the surface after laser ablation with different laser-pulse energies.

A. Shockwave expansion

Fig. 4(a) shows the spherical shockwaves with similar wave radius induced by four different pulse energies. The shockwave expands faster with increased pulse energy, accompanied with a larger plasma plume. The shockwave expansion is quantified by

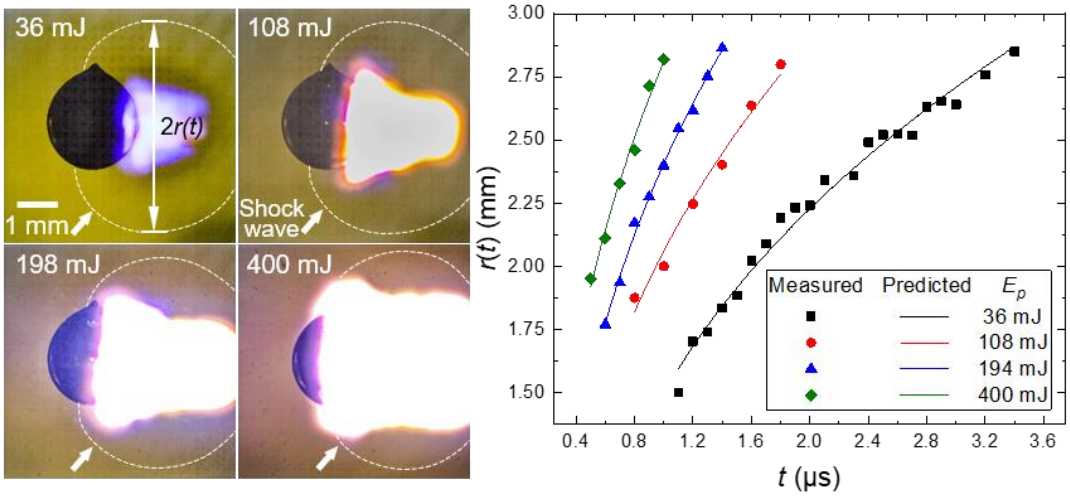

FIG. 4. (a) The shock wave with different laser-pulse energies; (b) Shockwave radius vs time.

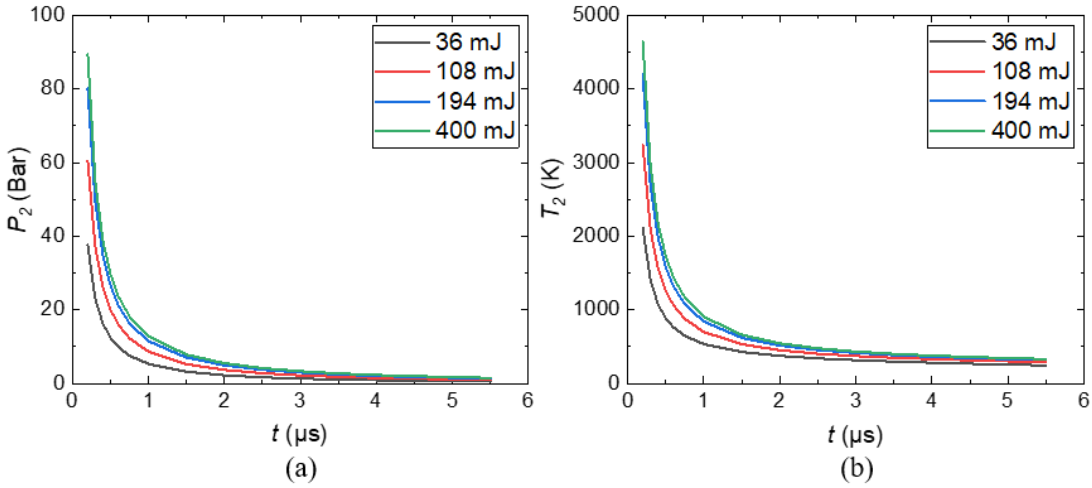

FIG. 5. The pressure and temperature of the shockwave with different laser-pulse energies.

the wave front radius $r(t)$, as shown in Fig. 4(a). The effective energy driving the shockwave can be obtained by employing Taylor's blast model[33]:

$$E = r\left(t\right)^5 \rho / t^2, \tag{2}$$

where E is the effective energy, ρ is the density of the air in front of the shockwave and t is the time after the laser pulse. This relation can be re-written in the form:

$$r\left(t\right) \sim \left(E/\rho\right)^{1/5} t^{2/5}. \tag{3}$$

A single parameter fit of Eq. (3) yields decent agreement with the experimental data [Fig. 4(b)]. We pointed out that the effective energy E used in Eq. (3) is less than the

injected laser pulse energy E_p (Table 1). There are two possible reasons for the difference between E and E_p. The first reason is the heat absorbed by the drop surface to cause the phase change (evaporation) of the liquid metal upon laser ablation. The second reason is that when the plasma reaches the critical density of the pump beam, significant reflection of the photons by the plasma occurs[11, 35], which can help explain that the effective energy E decreases to 248.6 mJ rapidly when the laser pulse energy E_p is 400 mJ.

Table 1. The effective energies (E) with different laser pulse energies (E_p).

E_p (mJ)	36	108	194	400
E (mJ)	28.6	93.7	189.9	248.6

In addition, the pressure and temperature behind the shockwave can be estimated by the classic shockwave equations[23]:

$$Ma = \frac{V_{sw}}{a} = \frac{V_{sw}}{\sqrt{\gamma R T_1}}, \tag{4}$$

$$\frac{P_2}{P_1} = 1 + \frac{2\gamma}{\gamma + 1}\left(Ma^2 - 1\right), \tag{5}$$

$$\frac{T_2}{T_1} = \frac{P_2}{P_1}\left(\frac{\frac{\gamma+1}{\gamma-1} + \frac{P_2}{P_1}}{1 + \frac{\gamma+1}{\gamma-1}\frac{P_2}{P_1}}\right), \tag{6}$$

where Ma is the Mach number, V_{sw} is the velocity of the shock wave, a is the speed of sound in air, γ is the specific heat ratio, R is the gas constant, P and T are the pressure and temperature respectively; the subscripts 1 and 2 represent the air in front of and behind the shockwave, respectively. Differential of Eq. (2) with respect to t gives the

shockwave expansion velocity:

$$V_{sw} \sim At^{-3/5}, \tag{7}$$

A is a function of energy and can be obtained by fitting the experimental data. The pressure behind the shockwave is obtained by Eq. (7) and Eq. (5):

$$\frac{P_2}{P_1} = 1 + \frac{2\gamma}{\gamma + 1}\left(\left(\frac{2/5\, At^{-3/5}}{a}\right)^2 - 1\right). \tag{8}$$

The temperature T_2 is calculated by Eq. (8) and Eq. (6). The results of pressure and temperature of the shockwave induced by laser pulses with different pulse energies are shown as solid curves in Fig. 5. The estimated pressure and temperature of the shockwave at t=1 μs are about 10 bar and 750 K, respectively. At t=5 μs, both the pressure and temperature behind shockwave restore the values of ambient air.

B. Time evolution of the drop deformation

The overall deformation of the drop is quantified by measuring the streamwise size of the concave W and the spanwise size of the drop L [Fig. 2(a)] over time with various pulse energies. A faster concave expansion [Fig. 6(a)] and more rapid spanwise depression [Fig. 6(b)] of the drop occur with higher pulse energy. Because W is a direct consequence of laser ablation and is clearly related to E_p and expands with time, we hypothesize that a length expansion scaling similar to the Taylor's blast model [Eq. (3)] may exist. We reorganized the data in Fig. 6(a) by plotting W against $(E_p/\rho_m)^{1/5}t^{-2/5}$, where ρ_m is the density of the liquid metal. Interestingly, all data for different E_p approximately collapses to a single straight line [Fig. 6(c)], supporting the notion that W scales with $E_p^{1/5}$. Note that the earlier data points are more scattered, possibly due to

the initial stage of material ejection and plasma formation. It has been reported that the laser ablated drop behaves similar to drop impact on a flat rigid surface[20], and the deformed drop can be described by a truncated sphere[36]. In other words, $W/2$ and $h=(D_0-L)$ are the radius and height of the spherical cap being removed [Fig. 2(a)]. If $h \ll D_0$, then $h \approx W^2/(4D_0)$, or h scales with $(E_p/\rho_m)^{2/5}t^{-4/5}$. Indeed, when Fig. 6(b) is replotted as L vs. $(E_p/\rho_m)^{2/5}t^{-4/5}$, again, all data for different E_p approximately collapses to a single straight line [Fig. 6(d)].

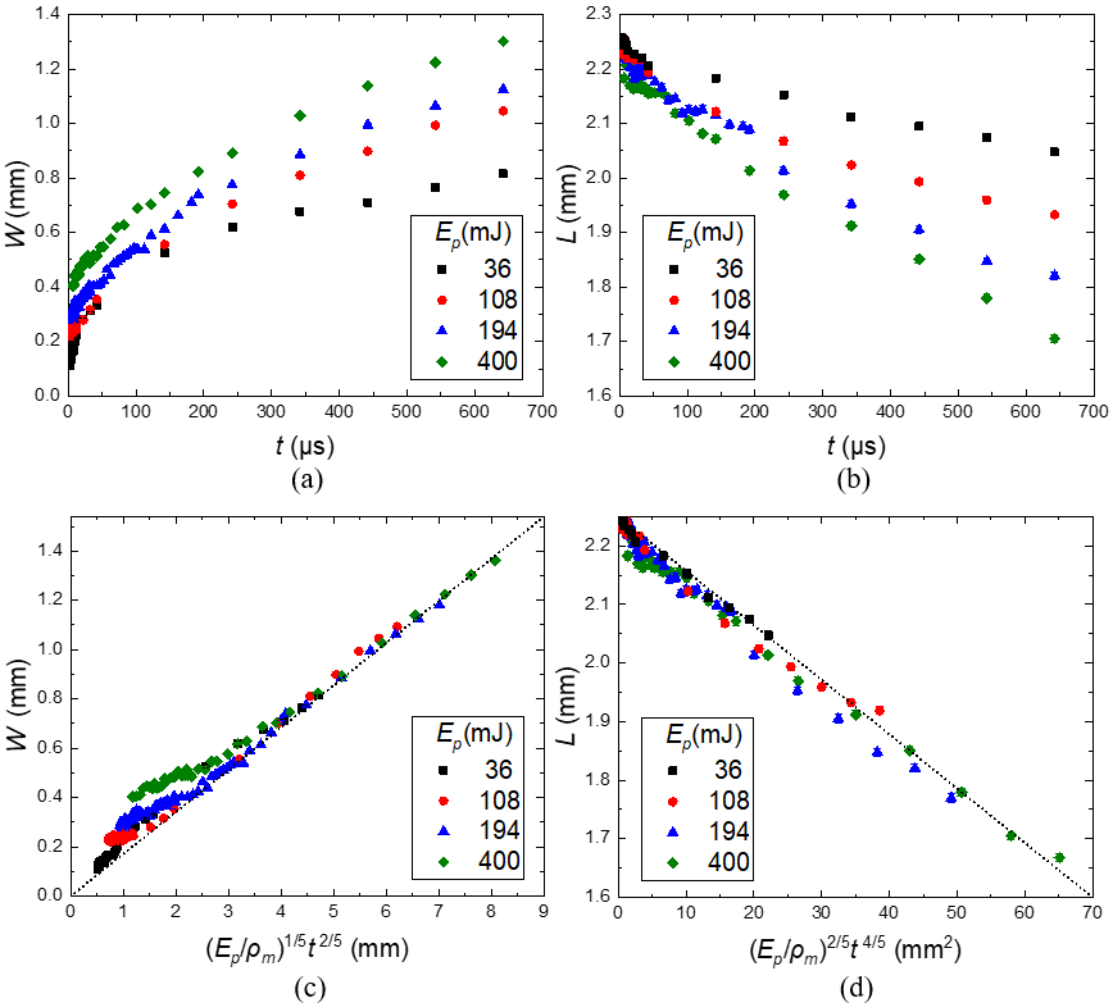

FIG. 6. (a)(b) The streamwise size of the concave W and the spanwise size of the drop in the center L after laser ablation with different laser-pulse energies; (c)(d) Collapse of W and L over time for all laser-blast induced drop deformation with different laser-pulse energies.

C. Lateral drop motion

The lateral drop motion is defined by the displacement of the mass center X of the drop during the first few milliseconds after the laser ablation. Fig. 7(a) shows the drop is accelerated to a constant speed U that increases with higher laser pulse energy, despite a significant deformation of the drop. The velocity of the drop ranges from 0.028 m/s to about 0.11 m/s with various laser pulse energy, following a power-law scaling with E_p [Fig. 7(b)]. The lateral drop motion scaling of the laser ablation with liquid metal droplet has been extensively studied by Kurilovich et al.[32], who developed a semi-empirical formula:

$$U = B\left(E_p - E_{od,0}\right)^{\alpha}, \tag{9}$$

where B is a proportionality constant, $E_{od,0}$ is an offset pulse energy determined by the laser/metal interaction, α is the power constant. Upon the laser impacting the drop (mass M), a plasma (mass m) with a velocity of v is generated, which propels the drop into lateral motion. The momentum conservation $MU = mv$ and a semi-empirical mass ablation law[15, 16] yield:

$$U = K\left[\left(\frac{I}{10^{11}\ \mathrm{W/cm^2}}\right)^{5/9}\left(\frac{\lambda}{1\ \mu\mathrm{m}}\right)^{-4/9} Z^{3/8}\right] S\tau_p v / M, \tag{10}$$

where I is the laser-pulse intensity, λ is the wavelength, Z is the average atomic number $Z \simeq 36.4$ (for 70Ga-30In); S is the area of the focal point. This relation predicts a power-law $U \propto I^{\alpha} \propto E^{\alpha}$ with α=5/9. The offset energy is determined by the laser fluence of the onset of the plasma formation upon the laser ablating the metal $F_{th} = \rho_m \Delta H \sqrt{\kappa \tau_p}$, as well as the reflectivity Γ of the surface[39] when the inverse bremsstrahlung is not yet

dominant as the pulse energy decreases, which gives:

$$E_{od,0} = S\rho_m \Delta H \sqrt{\kappa \tau_p} \big/ (1-\Gamma). \tag{11}$$

Here, with the latent heat of vaporization $\Delta H \approx 3.16\ \mathrm{MJ \cdot kg^{-1}}$ and thermal diffusivity $\kappa \approx 27.0\ \mathrm{mm^2 \cdot s^{-1}}$, we obtain $E_{od,0} = 41.27\ \mathrm{mJ}$. The result of a single constant fitting of Eq. (9) to the full energy range of experimental data yields decent agreement [Fig. 7(b)], from which we obtain $B = 0.00408\ \mathrm{m \cdot s^{-1} \cdot mJ^{-5/9}}$. Therefore, the scaling (9) describes all our experimental data well, which extends the applicable range of the original propulsion speed scaling from a few tens of micrometers to the capillary length (~ 2 mm in diameter).

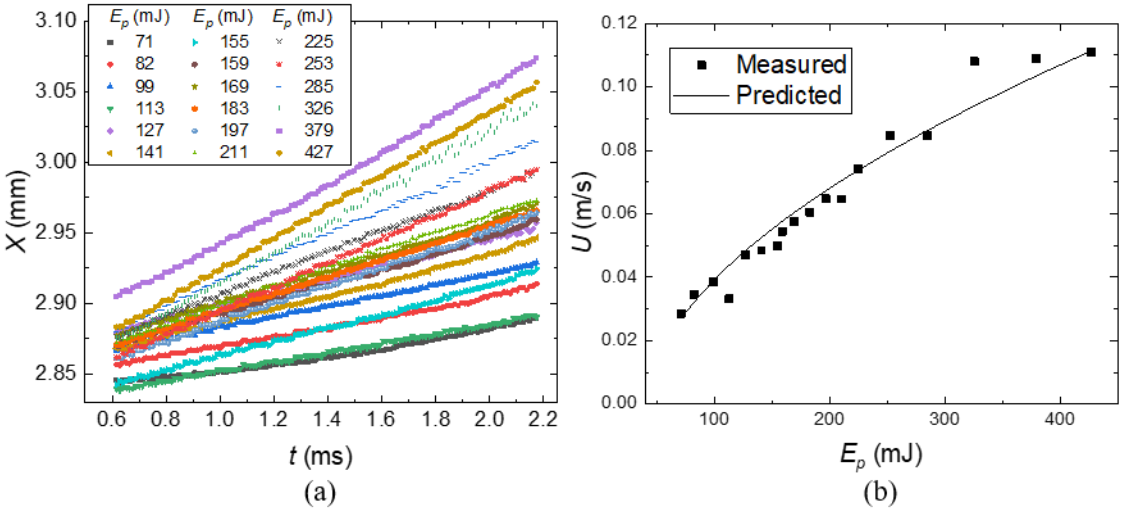

FIG. 7. (a) The drop mass center displacement X varying with time; (b) Measured propulsion velocity of the drop as a function of the laser pulse energy E_p. The solid line represents a fit of Eq. (9) to the concatenated data for the full range.

IV. Conclusions

We experimentally studied a millimeter-sized liquid metal drop ablated by an intense Nd: YAG laser pulse of 36 to 400 mJ pulse energy. The rapid drop deformation

was captured by timed delayed stroboscopic shadowgraph. The shockwave expansion in air was visualized, and the effective energy can be obtained via Taylor's blast model. The laser-blast-induced drop concave expansion and spanwise depression data collapse on straight lines with proper rescaling of pulse energy and time. The power law of propulsion speed by laser oblation of an In-Sn droplet of tens of micrometers can be extended to describe the laser-blast propelled motion of a millimeter-sized Ga-In drop.

Acknowledgements

This work was supported by the China Postdoctoral Science Foundation (Grant No. 2021M691426) and the National Natural Science Foundation of China (No. 11872199).

References

1. S. Y. Grigoryev, B. V. Lakatosh, M. S. Krivokorytov, V. V. Zhakhovsky, S. A. Dyachkov, D. K. Ilnitsky, K. P. Migdal, N. A. Inogamov, A. Y. Vinokhodov, V. O. Kompanets, Y. V. Sidelnikov, V. M. Krivtsun, K. N. Koshelev, and V. V. Medvedev, "Expansion and Fragmentation of a Liquid-Metal Droplet by a Short Laser Pulse," Physical Review Applied **10**, (2018).

2. V. M. Boiko, and S. V. Poplavski, "Experimental study of two types of stripping breakup of the drop in the flow behind the shock wave," Combustion, Explosion, and Shock Waves **48**, 440 (2012).

3. D. Ursescu, V. Aleksandrov, D. Matei, I. Dancus, M. D. de Almeida, and C. A. Stan, "Generation of shock trains in free liquid jets with a nanosecond green laser," Physical Review Fluids **5**, 123402 (2020).

4. A. Casner, C. Mailliet, G. Rigon, S. F. Khan, D. Martinez, B. Albertazzi, T. Michel, T. Sano, Y. Sakawa, P. Tzeferacos, D. Lamb, S. Liberatore, N. Izumi, D. Kalantar, P. Nicola, J. M. Nicola, E. Bel, I. Igumenshchev, and M. Koenig, "From ICF to laboratory astrophysics: Ablative and classical Rayleigh-Taylor instability experiments in turbulent-like regimes," Nuclear Fusion **59**, 032002 (2019).

5. V. Gopalaswamy, R. Betti, J. P. Knauer, N. Luciani, D. Patel, K. M. Woo, A. Bose, I. V. Igumenshchev, E. M. Campbell, K. S. Anderson, K. A. Bauer, M. J. Bonino, D. Cao, A. R. Christopherson, G. W. Collins, T. J. B. Collins, J. R. Davies, J. A. Delettrez, D. H. Edgell, R. Epstein, C. J. Forrest, D. H. Froula, V. Y. Glebov, V. N. Goncharov, D. R. Harding, S. X. Hu, D. W. Jacobs-Perkins, R. T. Janezic, J. H. Kelly, O. M. Mannion, A. Maximov, F. J. Marshall, D. T. Michel, S. Miller, S. F. B. Morse, J. Palastro, J. Peebles, P. B. Radha, S. P. Regan, S. Sampat, T. C. Sangster, A. B. Sefkow, W. Seka, R. C. Shah, W. T. Shmyada, A. Shvydky, C. Stoeckl, A. A. Solodov, W. Theobald, J. D. Zuegel, M. G. Johnson, R. D. Petrasso, C. K. Li, and J. A. Frenje, "Tripled yield in direct-drive laser fusion through statistical modelling," Nature **565**, 581 (2019).

6. J. P. Sauppe, S. Palaniyappan, B. J. Tobias, J. L. Kline, K. A. Flippo, O. L. Landen, D. Shvarts, S. H.

Batha, P. A. Bradley, E. N. Loomis, N. N. Vazirani, C. F. Kawaguchi, L. Kot, D. W. Schmidt, T. H. Day, A. B. Zylstra, and E. Malka, "Demonstration of Scale-Invariant Rayleigh-Taylor Instability Growth in Laser-Driven Cylindrical Implosion Experiments," Physics Review Letter **124**, 185003 (2020).
7. G. Terrones, and T. Heberling, "Rayleigh–Taylor instability at spherical interfaces between viscous fluids: The fluid/fluid interface," Physics of Fluids **32**, 094105 (2020).
8. J. Ding, L. Yu, M. Chen, Z. Zhai, T. Si, and X. Luo, "Interaction of planar shock wave with three-dimensional heavy cylindrical bubble," Physics of Fluids **30**, 106109 (2018).
9. R. Schupp, L. Behnke, J. Sheil, Z. Bouza, M. Bayraktar, W. Ubachs, R. Hoekstra, and O. O. Versolato, "Characterization of 1- and 2−μm-wavelength laser-produced microdroplet-tin plasma for generating extreme-ultraviolet light," Physical Review Research **3**, 013294 (2021).
10. R. Schupp, F. Torretti, R. A. Meijer, M. Bayraktar, J. Scheers, D. Kurilovich, A. Bayerle, K. S. E. Eikema, S. Witte, W. Ubachs, R. Hoekstra, and O. O. Versolato, "Efficient Generation of Extreme Ultraviolet Light From Nd:YAG-Driven Microdroplet-Tin Plasma," Physical Review Applied **12**, 014010 (2019).
11. S. Amoruso, R. Bruzzese, N. Spinelli, and R. Velotta, "Characterization of laser-ablation plasmas," Journal of Physics B Atomic Molecular & Optical Physics **32**, R131 (1999).
12. E. G. Gamaly, A. V. Rode, B. Luther-Davies, and V. T. Tikhonchuk, "Ablation of solids by femtosecond lasers: Ablation mechanism and ablation thresholds for metals and dielectrics," Physics of Plasmas **9**, 949 (2002).
13. B. N. Chichkov, C. Momma, S. Nolte, F. von Alvensleben, and A. Tünnermann, "Femtosecond, picosecond and nanosecond laser ablation of solids," Applied Physics A **63**, 109 (1996).
14. Gamaly, G. E., Rode, V. A., Tikhonchuk, T. V., and Luther-Davies, "Ablation of solids by femtosecond lasers: ablation mechanism and ablation thresholds for metals and dielectrics," Phys.Rev.A (2001).
15. R. A. Burdt, S. Yuspeh, K. L. Sequoia, Y. Tao, M. S. Tillack, and F. Najmabadi, "Experimental scaling law for mass ablation rate from a Sn plasma generated by a 1064 nm laser," Journal of Applied Physics **106**, (2009).
16. S. S. Harilal, T. Sizyuk, A. Hassanein, D. Campos, P. Hough, and V. Sizyuk, "The effect of excitation wavelength on dynamics of laser-produced tin plasma," Journal of Applied Physics **109**, (2011).
17. S. Donadello, V. Finazzi, A. G. Demir, and B. Previtali, "Time-resolved quantification of plasma accumulation induced by multi-pulse laser ablation using self-mixing interferometry," Journal of Physics D Applied Physics **53**, 495201 (2020).
18. M. M. Basko, V. G. Novikov, and A. S. Grushin, "On the structure of quasi-stationary laser ablation fronts in strongly radiating plasmas," Physics of Plasmas **22**, (2015).
19. A. Klein, C. W. Visser, W. Bouwhuis, H. Lhuissier, C. Sun, J. Snoeijer, E. Villermaux, D. Lohse, and H. Gelderblom, "Laser impact on a drop," Physics of Fluids **27**, 091106 (2015).
20. H. Gelderblom, H. Lhuissier, A. Klein, W. Bouwhuis, D. Lohse, E. Villermaux, and J. Snoeijer, "Drop deformation by laser-pulse impact," Journal of Fluid Mechanics **794**, 676 (2016).
21. A. L. Klein, D. Kurilovich, H. Lhuissier, O. O. Versolato, D. Lohse, E. Villermaux, and H. Gelderblom, "Drop fragmentation by laser-pulse impact," Journal of Fluid Mechanics **893**, (2020).
22. N. Bremond, and E. Villermaux, "Bursting thin liquid films," Journal of Fluid Mechanics **524**, 121 (2005).
23. S. R. Gonzalez Avila, and C.-D. Ohl, "Fragmentation of acoustically levitating droplets by laser-induced cavitation bubbles," Journal of Fluid Mechanics **805**, 551 (2016).

24. D. Kurilovich, M. M. Basko, D. A. Kim, F. Torretti, R. Schupp, J. C. Visschers, J. Scheers, R. Hoekstra, W. Ubachs, and O. O. Versolato, "Power-law scaling of plasma pressure on laser-ablated tin microdroplets," Physics of Plasmas **25**, (2018).
25. D. Kurilovich, T. D. F. Pinto, F. Torretti, R. Schupp, J. Scheers, A. S. Stodolna, H. Gelderblom, K. S. E. Eikema, S. Witte, W. Ubachs, R. Hoekstra, and O. O. Versolato, "Expansion Dynamics after Laser-Induced Cavitation in Liquid Tin Microdroplets," Physical Review Applied **10**, 054005 (2018).
26. B. Liu, D. Kurilovich, H. Gelderblom, and O. O. Versolato, "Mass Loss from a Stretching Semitransparent Sheet of Liquid Tin," Physical Review Applied **13**, 024035 (2020).
27. S. A. Reijers, J. H. Snoeijer, and H. Gelderblom, "Droplet deformation by short laser-induced pressure pulses," Journal of Fluid Mechanics **828**, 374 (2017).
28. S. T. Thoroddsen, K. Takehara, T. G. Etoh, and C. D. Ohl, "Spray and microjets produced by focusing a laser pulse into a hemispherical drop," Physics of Fluids **21**, (2009).
29. J. Hermens, H. Gelderblom, B. Liu, J. Duffhues, P. Rindt, and O. O. Versolato, "Laser-impact-induced splashing: an analysis of the splash crown evolution after Nd:YAG ns-pulse laser impact on a liquid tin pool," Applied Physics B **127**, (2021).
30. A. Klein, W. Bouwhuis, C. W. Visser, H. Lhuissier, C. Sun, J. Snoeijer, E. Villermaux, D. Lohse, and H. Gelderblom, "Drop Shaping by Laser-Pulse Impact," Physical Review Applied **3**, 044018 (2015).
31. A. L. Klein, D. Lohse, M. Versluis, and H. Gelderblom, "Apparatus to control and visualize the impact of a high-energy laser pulse on a liquid target," Rev Sci Instrum **88**, 095102 (2017).
32. D. Kurilovich, A. L. Klein, F. Torretti, A. Lassise, R. Hoekstra, W. Ubachs, H. Gelderblom, and O. O. Versolato, "Plasma Propulsion of a Metallic Microdroplet and its Deformation upon Laser Impact," Physical Review Applied **6**, 014018 (2016).
33. G. Taylor, "The Formation of a Blast Wave by a Very Intense Explosion. II. The Atomic Explosion of 1945," Proceedings of the Royal Society of London. Series A, Mathematical and Physical Sciences **201**, 175 (1950).
34. R. Fabbro, J. Fournier, P. Ballard, D. Devaux, and J. Virmont, "Physical study of laser‐produced plasma in confined geometry," Journal of Applied Physics **68**, 775 (1990).
35. D. Campos, S. S. Harilal, and A. Hassanein, "The effect of laser wavelength on emission and particle dynamics of Sn plasma," Journal of Applied Physics **108**, (2010).
36. W. Bouwhuis, R. C. van der Veen, T. Tran, D. L. Keij, K. G. Winkels, I. R. Peters, D. van der Meer, C. Sun, J. H. Snoeijer, and D. Lohse, "Maximal air bubble entrainment at liquid-drop impact," Phys Rev Lett **109**, 264501 (2012).
37. G. Jezequel, J. Lemonnier, and J. Thomas, "Optical properties of gallium films between 2 and 15 eV," Journal of Physics F: Metal Physics **7**, 1613 (1977).
38. R. Y. Koyama, N. V. Smith, and W. E. Spicer, "Optical Properties of Indium," Physical Review B **8**, 2426 (1973).
39. The reflectivity for pure gallium is $\Gamma = 80\%$ (from Ref. [37] at 4 eV at 88 K). For indium, a reflectivity of $\Gamma = 91\%$ is obtained from $n = 1.84$ and $k = 8.38$ (from Ref. [38] at 1.1 μm at 295 K). An estimate of the eutectic optical response is obtained from the averaging the reflectivities, yielding an absorption $1 - \Gamma = 17\%$.